

The Journal of Neuroscience

<http://jneurosci.msubmit.net>

JN-BC-3640-14R2

Neural mechanisms for discounting head-roll-induced retinal motion

Andrew Smith, Royal Holloway, University of London
Jac Billington, University of Leeds

Commercial Interest: No

1 (second revision, 15 Jan 2015)

2

3 **Neural mechanisms for discounting head-roll-induced retinal motion**

4

5 **Jac Billington¹ & Andrew T Smith**

6

7 Department of Psychology, Royal Holloway, University of London,

8 Egham, TW20 0EX, UK

9

10 ¹ Present address: Institute of Psychological Sciences, University of Leeds,

11 Leeds, LS2 9JT, UK

12

13

14 Corresponding author: Andy Smith (a.t.smith@rhul.ac.uk)

15

16 Abbreviated title: Discounting head-roll-induced motion

17 Word counts: Abstract 190, Introduction 489, Discussion 850, Total 4492

18 Number of figures: 4. Number of pages: 19. No tables, multimedia or 3D models.

19 Conflicts of interest: none

20

21 Acknowledgement: Supported by a grant from the Leverhulme Trust to ATS

22

23 **Abstract**

24

25 An extensive series of physiological studies in macaques shows the existence of neurons
26 in three multisensory cortical regions, MSTd, VIP and VPS, that are tuned for direction
27 of self-motion in both visual and vestibular modalities. Some neurons have congruent
28 direction preferences, suggesting integration of signals for optimum encoding of self-
29 motion trajectory; others have opposite preferences and could be used for discounting
30 retinal motion that arises from perceptually irrelevant head motion. Whether such a
31 system exists in humans is unknown. Here, artificial vestibular stimulation was elicited
32 in human participants during fMRI scanning in conjunction with carefully calibrated
33 visual stimulation that emulated either congruent or opposite stimulation conditions.
34 Direction and speed varied sinusoidally such that the two conditions contained identical
35 vestibular stimulation and identical retinal stimulation, differing only in the relative
36 phase of the two components. In human MST (hMST) and putative VIP (pVIP), multi-
37 voxel pattern analysis (MVPA) permitted classification of stimulus phase based on fMRI
38 time-series data, consistent with the existence of separate neuron populations
39 responsive to congruent and opposite cue combinations. Decoding was also possible in
40 the vicinity of parieto-insular vestibular cortex (PIVC), possibly in a homologue of
41 macaque VPS.

42

43

44

45 **Introduction**

46

47 Moving successfully through the environment requires the integration of visual and
48 vestibular information. These senses provide primary sources of information for
49 determining our own inertia and (in the case of vision) the movement of objects in the
50 environment. However, natural movements of the head during self-motion result in
51 optic flow that confounds both visual heading perception and detection of object
52 motion. Multisensory integration potentially provides a means by which irrelevant
53 retinal motion arising from the movement of the body, eyes and head can be discounted
54 from retinal motion that occurs as a result of either self-translation or movement of
55 external objects.

56

57 Physiological studies of the integration of visual and vestibular cues have implicated
58 macaque dorsal medial superior temporal area MSTd (Gu et al., 2006) and ventral
59 intraparietal area VIP (Chen et al., 2011a); see Fetsch et al. (2013) for review. In these
60 cortical regions, some neurons have congruent visual-vestibular preferences for
61 direction of translation (heading) and others, in similar numbers, have opposite
62 preferences. A third region, the visual posterior sylvian area VPS, has many neurons
63 with opposite preferences, although few with congruent preferences (Chen et al.,
64 2011b). Neurons with congruent and opposite preferences may serve to strengthen the
65 perception of heading and to discount optic flow that arises from head-motion,
66 respectively. During rotational motion, VIP shows similar proportions of neurons with
67 opposite and congruent visual-vestibular preference (Chen et al., 2011a), but MSTd
68 shows a marked predominance of neurons with opposite preferences (Takahashi et al.,
69 2007). This predominance might suggest that rotational vestibular cues resulting from

70 head motion are encoded in MSTd primarily for the purpose of distinguishing relevant
71 external motion from irrelevant self-motion. Whole-field visual flow can be used for this
72 purpose but the additional use of vestibular cues might increase precision and also
73 potentially disambiguates head rotation from large rotating objects.

74

75 In human neuroimaging studies, several cortical regions show specificity for optic flow,
76 including a region known as hMST, which may include a homologous region to macaque
77 MSTd. The cingulate sulcus visual area (CSv) and a region in intraparietal cortex that
78 has some characteristics in common with macaque VIP (putative human VIP or pVIP),
79 have been shown to favor optic flow that reflects self-motion over flow that does not
80 (Wall and Smith, 2008; Cardin and Smith, 2010). hMST and CSv have also been found to
81 respond to vestibular stimulation (Smith et al., 2012). Whether any of these areas
82 contain neurons capable of disambiguating relevant and irrelevant visual cues by the
83 use of opposite visual-vestibular preferences is unknown.

84

85 Standard artificial methods of inducing vestibular sensation in a scanner environment
86 result in visual sensations that are inconsistent with natural visual-vestibular cue
87 combinations, making meaningful study of visual-vestibular interactions very difficult.
88 Using psychophysics, we were able to emulate cue combinations compatible with
89 natural head roll by employing visual stimuli that were tailored to match the measured
90 sensation of head roll induced by galvanic vestibular stimulation (GVS). We then used
91 multivariate pattern analysis to determine whether distinct populations of congruent
92 and opposite neurons exist in human cortical regions that are known to be involved in
93 multisensory processing.

94

95 **Materials and Methods**

96

97 *Participants:* Seven healthy participants (5 female, median age 20 years) took part. They
98 were screened according to standard procedures and gave informed consent. The study
99 was approved by the relevant local ethics committee.

100

101 *Stimuli:* During GVS, sinusoidal waveforms were used to generate vestibular stimulation
102 with an isolated bipolar constant-current stimulator (DS5, Digitimer Ltd) located in the
103 scanner control room. Stimulation was delivered via shielded cables that were passed
104 through appropriate RF filters into the MRI examination room. Non-metallic electrodes
105 (Skintact F-WA00, Leonhard Lang Ltd) were placed over the mastoid bone just behind
106 each ear. A sinusoidal alternating current (1Hz, $\pm 3\text{mA}$) passed between the two
107 electrodes, activating the cranial nerves connecting the vestibular organs to the
108 brainstem. This induced a perception of head roll (rotation, R, about the anterior-
109 posterior head axis). The magnitude (excursion, in degrees) of perceived roll induced by
110 vestibular activation is referred to here as R_{vest} . GVS also induces a vestibulo-ocular
111 reflex with a dominant torsional component, R_{vor} . This causes rotation of the image on
112 the retina (R_{ret_vor}) which is equal in magnitude but opposite in direction to R_{vor} and
113 affects visual cues to head roll.

114

115 Visual stimuli were presented to the participant via a NordicNeuroLab VisualSystem.
116 This is an optical goggle system, chosen because it allowed the surroundings (scanner
117 bore, etc.) to be completely occluded, by the lens hoods. The system included an IR
118 video camera (60Hz) for monitoring eye movements. The IR image was processed with

119 software (Arrington, Inc) that could detect cyclotorsional eye rotation, based on the
120 features of the iris, as well as gaze direction. The image presented was dark apart from
121 2000 white dots (limited lifetime to reduce afterimages, 120/sec replaced) in a circular
122 patch of diameter 15deg. The patch could be rotated sinusoidally about its center, at a
123 rate and phase that matched the sinusoidal percept induced by GVS. The phase differed
124 from the GVS waveform by 90 deg to account for the integration of acceleration to speed
125 seen in vestibular responses at 1Hz (e.g. Fernandez and Goldberg, 1971). The
126 magnitude of rotation could be varied. It was found that if the magnitude was
127 appropriate, the sensation of visual roll induced by GVS could be nulled so that the dot
128 patch appeared static (see *Pre-scan calibrations*). During periods with no GVS, the dot
129 patch remained present but was stationary. The dot patch contained a central fixation
130 point that changed randomly among 5 possible colors at 2Hz. Participants engaged in a
131 color counting task that encouraged good fixation and maintained attention in a
132 constant state.

133

134 *Pre-scan calibrations:* Prior to the main experimental runs, each participant carried out
135 two short procedures in the scanner to obtain session-tailored calibration values for the
136 fMRI experiment. These values vary across individuals and sessions so it was important
137 to obtain measures in the same session as the scan. First, a psychophysical nulling
138 calibration determined R_{screen_null} , the extent to which the dot patch had to rotate in
139 order to null the perception of roll motion (R_{perc}) created by GVS. Participants fixated
140 the central target and received 1sec of GVS. They then pressed one of two buttons to
141 indicate whether they perceived clockwise (CW) or anticlockwise (ACW) rotation of the
142 visual stimulus. Image rotation was then varied over trials with a Best-PEST staircase

143 procedure (Lieberman and Pentland, 1982) to find the best value of R_{screen_null} . This
144 value was then tested, by giving the participant several 16sec GVS stimulations to
145 induce CW R_{perc} , at the same time rotating the dot patch ACW by R_{screen_null} . We were
146 satisfied that an adequate null had been achieved if participants could not perceive
147 motion or could not follow the direction of motion. The measured value of R_{screen_null}
148 was then used in the Nulled condition of the fMRI experiment (see *Conditions* below) for
149 that participant. It was found that on average the dot patch had to rotate sinusoidally
150 $\pm 1.71^\circ$ (sd=0.51, min=0.75, max=2.65) in order to cancel the percept of motion induced
151 by the GVS.

152

153 Second, GVS was administered in blocks of 16s (six blocks separated by 8s rest blocks)
154 while cyclotorsional eye position was tracked, in order to measure R_{vor} . R_{vor} is always
155 in the opposite direction to R_{perc} , the purpose of VOR being to compensate for head
156 motion. Participants fixated and passively viewed the static dot patch. They were
157 presented with 12 blocks (16secs) of GVS and torsional eye traces were recorded. At the
158 end of the calibration the eye data were smoothed and the amplitude of cycles 4-12 was
159 extracted and averaged across cycles and blocks. This was 0.43° on average (sd = 0.14,
160 min=0.16, max=0.62; this low VOR gain is typical of previous studies). The participant-
161 specific value measured was used to adjust the retinal speed of the Control condition
162 (see *Conditions*) so as to match that of the Nulled condition i.e. to compensate for the
163 effect of R_{vor} on retinal motion.

164

165 *Conditions:* Using the parameters obtained immediately prior to scanning, GVS was
166 applied together with visual rotation of a magnitude and direction that either cancelled
167 the percept induced by GVS (Nulled condition) or had the opposite phase, effectively
168 summing the retinal and vestibular effects (Control condition). The measured R_{vor}
169 parameter was used to equate retinal speed across the two conditions. A small
170 optokinetic reflex (OKR) may also have occurred but this was ignored because it would
171 be the same in both conditions, the retinal speed being the same.

172

173 Fig. 1 illustrates the two conditions quantitatively. The Nulled condition emulates
174 natural head roll, in which retinal motion is present (but is not perceived as rotation of
175 the visual world) and the visual and vestibular cues are congruent. In the Control
176 condition, GVS is the same but retinal motion reverses direction, the motion is strongly
177 perceived, and the two cues are incongruent (opposite in direction).

178

179 *Design:* The fMRI experiment employed a block design and consisted of eight ~5min
180 runs. 16s trial blocks were separated by 8s rest blocks and the two conditions were
181 each presented six times per run. This gave a total of 48 presentations per condition.
182 fMRI data were collected with a Siemens Trio 3-Tesla scanner with either an eight-
183 channel head array coil for acquisition of a high quality T1 weighted structural image
184 (MDEFT; Deichmann et al., 2004) or a custom 8-channel posterior head coil (Stark
185 Contrast, Germany) for an in-session T1 image and the functional images. Functional
186 images were collected with 23 oblique slices (2.5 mm isotropic voxels) with an
187 echoplanar imaging sequence (TR = 2 sec, TE = 33 msec).

188

189 *Analysis:* Both standard (univariate) analysis and multi-voxel pattern analysis (MVPA)
190 were used. Univariate analysis was carried out with BrainVoyager software (Goebel et
191 al., 2006). All functional data underwent preprocessing in which images were corrected
192 for slice timing and for head motion. High pass temporal filtering (cutoff 0.01Hz) was
193 used to remove low-frequency drifts. Functional data were co-registered to the MDEFT
194 anatomy. Statistical contrasts were set up using the general linear model to fit each
195 voxel timecourse with a model derived by convolving a standard haemodynamic
196 response function with the stimulus time series. Six additional regressors to model head
197 movements and a session regressor were added.

198

199 *Region of interest (ROI) analysis:* Various ROIs were defined in separate scans. hMST was
200 defined using a standard paradigm (Huk et al., 2002) based on the presence of
201 ipsilateral responses. Alternately expanding and contracting dot patterns (5deg
202 diameter; 13.5° eccentricity) were presented separately in the left or right visual
203 hemifields. 16s stimulus blocks were interleaved with blocks with static dots. CSv and
204 pVIP were defined using a second localiser (Wall and Smith, 2008) that consisted of two
205 conditions presented for 15s each, separated by 15s blocks with no stimulus. In one
206 condition, self-motion-compatible optic flow simulating spiral motion of the observer
207 was presented. The second condition contained locally matched dot motion but in a self-
208 motion-incompatible 3x3 array of 9 flow patches. Contrasting activity for compatible vs.
209 incompatible flow readily defined CSv. It also revealed a visually responsive region in
210 the vicinity of PIVC (see Cardin and Smith, 2010) that we refer to here as PIC (posterior
211 insular cortex) in line with previous studies. It is plausible that PIC is a homologue of
212 macaque VPS (Frank et al, 2014). In many cases, pVIP was also defined. We find that
213 pVIP is the most difficult region to define with this method because it responds quite

214 well to both stimuli and definition relies on a modest degree of differential activity. In a
215 few cases pVIP could not be defined reliably for this reason and in some others the
216 acquisition volume did not extend sufficiently far dorsally. V1 was also localised, to
217 provide a control ROI which was not expected to distinguish congruent and opposite
218 vestibular-visual cues. V1 was defined using standard retinotopic mapping procedures,
219 with a wedge (24° segment with a radius of 12°) rotating at 64 sec/cycle.

220

221 In addition to these visually defined ROIs, a vestibular localiser was used to determine
222 independent regions that responded to GVS in darkness. The GVS localiser employed 2 s
223 (2 cycles) of a 1 Hz sinusoid. Stimulation was followed by a 2-10 second inter-trial
224 interval. A total of 160 trials were presented across two runs. All light was excluded and
225 participants were also asked to close their eyes. Two ROIs were defined in this way.
226 PIVC was identified in all participants, in accord with several previous studies; however,
227 we refer here to the ROI defined in this way as PIVC/PIC because it likely includes PIC as
228 well as PIVC (see Discussion). Partial overlap was often seen between (vestibular)
229 PIVC/PIC and (visual) PIC but PIC was on average slightly more posterior (see Figure 2),
230 as is VPS in macaques. The proportion of overlapping voxels was 15%. A vestibular
231 hMST ROI was also identified bilaterally that overlapped with visually defined hMST but
232 was typically less extensive, in accord with previous work (Smith et al., 2012). The
233 overlap was 38%.

234

235 To test whether populations of neurons could distinguish the two cross-model
236 vestibular-visual cue combinations, the BOLD response in the main experiment was
237 extracted from all regions of interest and submitted to both univariate analysis as
238 above, to reveal any differences in response magnitude, and also to multi-voxel pattern

239 analysis (MVPA). MVPA was performed with a MATLAB-implemented LIBrary for
240 Support Vector Machines (LIBSVM; Chang and Lin, 2011). For each ROI, independently
241 and irrespective of overlap between visual and vestibular estimates of hMST and PIC,
242 the data were pooled across participants to create a single large sample and normalised
243 across the two conditions (see Furlan et al, 2014 for details of the method). Decoding
244 performance was measured as a function of the number of features (voxels) included,
245 which was incremented in steps of 30. The features were selected randomly. They were
246 resampled and the analysis repeated 5000 times at each increment. A leave-one-out
247 procedure was used to train a support vector machine (SVM) on 7 runs and test on the
248 remaining run, resulting in 8 performances for each sample. In order to test whether the
249 classifier was performing above chance, the analysis was re-run with random
250 permutation of trial labels. The 95th percentile of the distribution of 5000 results with
251 different randomly permuted labels was calculated in order to determine whether
252 correctly labelled classification analyses were performing significantly above chance.
253 The mean of the distribution was used to estimate chance performance (expected to be
254 50%).

255

256 **Results**

257

258 MVPA classification accuracies for decoding Nulled vs. Control within visually defined
259 hMST, pVIP, CSv and PIC, and vestibularly defined hMST and PIVC/PIC, are displayed in
260 Figure 3. Also included is V1, a control visual region that was not expected to distinguish
261 between Nulled and Control conditions. As the two conditions were matched for retinal
262 speed and GVS magnitude, decoding success is reliant on the presence of sensitivity to

263 the relative phase of the two signals, perhaps in the form of independent populations of
264 neurons that respond to congruent (Nulled condition) and opposite (Control condition)
265 head-roll cues.

266

267 Of the visually defined regions studied, hMST, pVIP and PIC all supported classification
268 of the two stimulus combinations, showing the expected increase in decoding
269 performance with the number of features included (illustrated only for hMST) and
270 reaching statistical significance for higher numbers of features. All three easily breached
271 the 95th percentile of the permuted data. The two conditions could not be significantly
272 decoded in visually defined CSv or in V1. Classification accuracy also reached
273 significance in the two ROIs defined vestibularly, PIVC/PIC and hMST.

274

275 The univariate magnitude of the BOLD response in each condition was extracted from
276 each ROI and is shown in Figure 4. All regions examined showed broadly comparable
277 responses in the two conditions, mirroring the matched retinal stimulation rather than
278 reflecting the difference in perceived motion resulting from the temporal phase in
279 which the stimuli were combined. There was an overall trend towards larger responses
280 in the Nulled condition (not significant by *t*-test in any region). A possible explanation of
281 this difference, if real, is that retinal motion in the Control condition was too weak.
282 Analysis of VOR gain showed that it was about 10% lower, in both conditions, than
283 during the pre-scan calibration on which the correction was based, which means that
284 retinal motion in the Control condition was somewhat slower than intended.

285

286 **Discussion**

287 Using psychophysics, we were able to create, and present to a static person lying in an
288 MRI scanner, visual-vestibular cue combinations that were consistent with natural head
289 rotation in the roll axis (congruent visual-vestibular cues). We were able to mimic the
290 natural situation in which the head rolls, the retinal image consequently rotates, but the
291 world appears static i.e. retinal image motion is suppressed. By reversing the direction
292 of retinal motion (to give opposite visual-vestibular cues) we could create a situation in
293 which the magnitude of retinal motion was unchanged but was now strongly perceived
294 because it summed with, rather than nulling, the effect of GVS (Control condition).
295 When direction of rotation was alternated over time by means of sinusoidal GVS
296 accompanied by sinusoidal retinal motion, each combination could be created in a
297 continuous fashion and we could switch between them by reversing the relative phase
298 of the two stimuli. The two conditions then contained identical retinal motion and
299 identical vestibular motion, and could be compared directly with fMRI, free from the
300 confound of absolute direction. This allowed us to determine whether several key brain
301 regions, some of which may be homologues of cortical regions in non-human primates
302 that have been shown to integrate visual and vestibular cues, were sensitive to the
303 difference between the two combinations i.e. to the relative phase in which the stimuli
304 were presented.

305

306 Univariate analysis of the fMRI data enabled us to ask, for each cortical region examined,
307 whether activity is determined by retinal motion or by perceived motion. The two
308 conditions elicited similar BOLD responses in all areas studied (Figure 4). Small
309 differences may exist that we failed to detect but activity appears to be broadly
310 governed by retinal motion rather than perceived motion. If anything, activity was
311 greater when no motion was visible (Nulled condition).

312

313 In contrast, multivariate analysis (MVPA) enabled us to distinguish the Nulled and
314 Control conditions in several cortical regions. First, hMST (whether defined with a
315 visual or vestibular localizer) displayed significant prediction accuracy, indicating that it
316 is sensitive to the phase in which visual and vestibular stimuli were combined. The most
317 obvious interpretation, given the physiological literature, is that hMST contains some
318 neurons that are selectively responsive to congruent visual/vestibular cues and others
319 that prefer opposite cues, although other interpretations are possible (e.g. a continuous
320 rather than bipolar distribution of phase sensitivities). If so, such neurons may act to
321 strengthen perception of heading and to identify and discount retinal motion that
322 results from head movements. The results incidentally provide further support for the
323 notion that hMST includes a sub-region that is homologous with macaque MSTd. The
324 fact that MSTd is driven more strongly by visual than vestibular input (Gu et al., 2006;
325 Takahashi et al., 2007; Chen et al., 2011b) and that the same is true of hMST (Smith et
326 al., 2012) is also consistent with this interpretation.

327

328 Areas pVIP and PIC also showed sensitivity to the phase of the visual and vestibular
329 stimuli, suggesting that they too may contain populations of neurons with congruent
330 and opposite preferences. This is consistent with a possible homology with macaque
331 areas VIP and VPS respectively. However considerable caution is needed here. In the
332 case of pVIP, the evidence for a functional homology is considerably weaker than for
333 hMST. Macaque VIP responds to both visual and vestibular heading cues (Bremmer et
334 al., 2002) and is involved in the integration of vestibular-visual information (Chen et al.,
335 2011a). The fact that human pVIP is also multisensory (Bremmer et al., 2001) fits well
336 with the possibility of a homology, as do the present results. However, the human

337 intraparietal sulcus (IPS) contains many more discrete sensory regions than macaque
338 IPS (e.g. Swisher et al., 2007) suggesting a different, more evolved organization. This
339 reduces the likelihood of direct functional equivalence. We use the acronym pVIP
340 because the area is the same as that referred to as human VIP by Bremmer et al., 2001,
341 not because we are confident of a homology. Cells with congruent and opposite heading
342 preferences have been found in VPS (Chen et al., 2011b), although with a
343 preponderance of oppositely tuned cells. PIVC/PIC defined with GVS supports pattern
344 classification. Macaque PIVC shows little responsiveness to optic flow but is prominent
345 in vestibular processing, and therefore may play a more peripheral role in multimodal
346 processing, perhaps by providing vestibular signals to VPS. It is therefore likely that
347 classification in vestibular PIVC/PIC was supported by neurons in the hypothesised PIC
348 portion of this ROI. CSv did not show predictor accuracy above chance, and whilst this
349 region has been found to respond well to vestibular as well as visual stimuli (Smith et
350 al., 2012), our results provide no evidence to suggest that it is involved in multisensory
351 integration.

352 In conclusion, our fMRI results, together with the finding that participants were unable
353 to see retinal motion when it emulated that which would be present in a typical head
354 roll situation, suggests that multisensory integration plays a large role in discounting
355 retinal motion that is irrelevant to interacting with the world and provides important
356 information concerning the locus of this process in the human brain.

357

358 **References**

359

360 Bremmer F, Klam F, Duhamel JR, Hamed SB, Graf W (2002) Visual-vestibular interactive
361 responses in the macaque ventral intraparietal area (VIP). *European Journal of*
362 *Neuroscience* 16:1569-1586.

363 Bremmer F, Schlack A, Shah N, Zafiris O, Kubischik M, Hoffmann K-P, Zillies K, Fink G
364 (2001) Polymodal motion processing in posterior parietal and premotor cortex:
365 a human fMRI study strongly implies equivalencies between humans and
366 monkeys. *Neuron* 29:287-296.

367 Cardin V, Smith AT (2010) Sensitivity of human visual and vestibular cortical regions to
368 egomotion-compatible visual stimulation. *Cerebral Cortex* 20:1964-1973.

369 Chang C-C, Lin C-J (2011) LIBSVM: a library for support vector machines *ACM*
370 *Transactions on Intelligent Systems and Technology* 2:21-27.

371 Chen A, DeAngelis GC, Angelaki DE (2010) Macaque Parieto-Insular Vestibular Cortex:
372 Responses to Self-Motion and Optic Flow. *Journal of Neuroscience* 30:3022-
373 3042.

374 Chen A, DeAngelis GC, Angelaki DE (2011a) Representation of Vestibular and Visual
375 Cues to Self-Motion in Ventral Intraparietal Cortex. *Journal of Neuroscience*
376 31:12036-12052.

377 Chen A, DeAngelis GC, Angelaki DE (2011b) Convergence of Vestibular and Visual Self-
378 Motion Signals in an Area of the Posterior Sylvian Fissure. *Journal of*
379 *Neuroscience* 31:11617-11627.

380 Deichmann R, Schwarzbauer C, Turner R (2004) Optimisation of the 3D MDEFT
381 sequence for anatomical brain imaging: technical implications at 1.5 and 3 T.
382 *NeuroImage* 21:757-767.

383 Fernandez C, Goldberg J (1971) Physiology of peripheral neurons innervating
384 semicircular canals of the squirrel monkey. II Response to sinusoidal stimulation
385 and dynamics of peripheral vestibular system. *Journal of Neurophysiology*
386 34:661-675.

387 Fetsch CR, DeAngelis GC, Angelaki DE (2013) Bridging the gap between theories of
388 sensory cue integration and the physiology of multisensory neurons. *Nature*
389 *Reviews Neuroscience* 14:429-442.

390 Frank SM, Baumann O, Mattingley JB, Greenlee MW (2014) Vestibular and visual
391 responses in human posterior insular cortex. *Journal of Neurophysiology* 112:
392 2481-2491.

393 [Furlan M, Wann JP, Smith AT \(2014\) A representation of changing heading direction in](#)
394 [human cortical areas pVIP and CSv. *Cerebral Cortex* 24:2848-2858.](#)

395 Goebel R, Esposito F, Formisano E (2006) Analysis of Functional Image Analysis Contest
396 (FIAC) data with BrainVoyager QX: From single-subject to cortically aligned
397 group general linear model analysis and self-organizing group independent
398 component analysis. *Human Brain Mapping* 27:392-401.

399 Gu Y, Watkins PV, Angelaki DE, DeAngelis GC (2006) Visual and Nonvisual Contributions
400 to Three-Dimensional Heading Selectivity in the Medial Superior Temporal Area.
401 *Journal of Neuroscience* 26:73-85.

402 Huk AC, Dougherty RF, Heeger DJ (2002) Retinotopy and functional subdivision of
403 human areas MT and MST. *Journal of Neuroscience* 22:7195-7205.

404 [Lieberman H, Pentland A \(1982\) Microcomputer based estimation of psychophysical](#)
405 [thresholds: the best PEST. *Behavioural Research Methods Instruments* 14:21-25.](#)

406 Smith AT, Wall MB, Thilo K (2012) Vestibular Inputs to Human Motion-Sensitive Visual
407 Cortex. *Cerebral Cortex* 22:1068-1077.

408 Swisher JD, Halko MA, Merabet LB, McMains SA, Somers DC (2007) Visual Topography
409 of Human Intraparietal Sulcus. *Journal of Neuroscience* 27:5326-5337.

410 Takahashi K, Gu Y, May PJ, Newlands SD, DeAngelis GC, Angelaki DE (2007) Multimodal
411 Coding of Three-Dimensional Rotation and Translation in Area MSTd:
412 Comparison of Visual and Vestibular Selectivity. *Journal of Neuroscience*
413 27:9742-9768.

414 Wall MB, Smith AT (2008) The representation of egomotion in the human brain. *Current*
415 *Biology* 18:191-194.

416
417
418

419 **Figure legends**

420 **Figure 1**

421 Quantitative example to illustrate stimulus construction. Positive values represent CW
422 movement, negative values ACW.

423 **(a)** GVS induces a CW vestibular head roll percept of say 2.5° ($R_{vest} = 2.5$). VOR acts to
424 stabilize the image: when the vestibular system signals CW head roll, which normally
425 causes ACW retinal motion, the eyes rotate ACW giving compensatory CW retinal
426 motion, say 0.5° ($R_{ret_vor} = 0.5$), which signals ACW head roll of -0.5° ($R_{head_vor} = -0.5$),
427 reducing the roll percept to 2.0° ($R_{perc} = 2.0$). Note that real CW head motion would make
428 the retinal image rotate ACW on the retina but in the case of GVS, the retinal image is
429 static (ignoring VOR), so you think the world (image) must be rotating CW.

430 **(b)** To cancel such a perceived rotation (Nulled condition), the dot patch must be
431 rotated in the opposite direction ($R_{screen_null} = -2.0$). This results in a nulled perceived roll
432 ($R_{perc} = 0$) and a retinal image rotation (R_{ret_null}) of -1.5° , the sum of R_{screen_null} and R_{ret_vor} .

433 **(c)** In the Control condition, retinal motion is required that is equal and opposite to the
434 Nulled condition ($R_{ret_ctrl} = 1.5$). The screen motion required to achieve this in the
435 presence of VOR ($R_{ret_vor} = 0.5$) is 1° ($R_{screen_ctrl} = 1.0$).

436

437 **Figure 2**

438 Flattened cortical representations from two participants. S1 and S2, showing the
439 Regions of Interest (ROIs) examined. Each ROI is shown as a color overlay (see key). V1,
440 hMST, pVIP, CSv and PIC defined by visual localisers are shown in addition to PIVC/PIC
441 and hMST defined with vestibular stimulation in darkness.

442

443 **Figure 3**

444 **(a)** MVPA classification accuracy for hMST, defined with a visual localizer, as a function
445 of the number of features included. Dashed portion of curve is extrapolated. **(b)** Peak
446 classification accuracy for all cortical regions examined, together with the associated
447 number of voxels in each case. Also shown are chance performance and the 95th
448 percentile from permutation testing (mean across all regions).

449

450 **Figure 4**

451 Mean BOLD response amplitudes (normalized percent signal change) for the Nulled and
452 Control conditions in each cortical region studied. Error bars show ± 1 SEM.

453

$R_{\text{vest}} = 2.5$



$R_{\text{head_vor}} = -0.5$



+

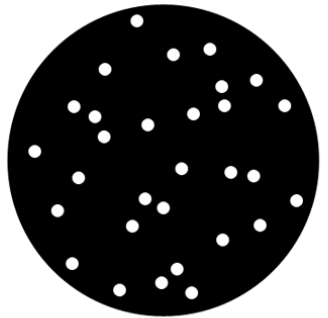
=

$R_{\text{perc}} = 2.0$



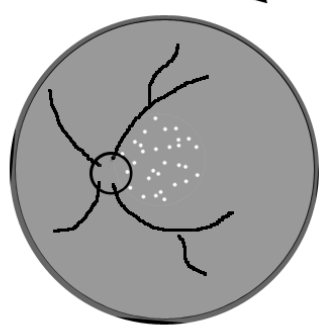
a

$R_{\text{screen_null}} = -2.0$



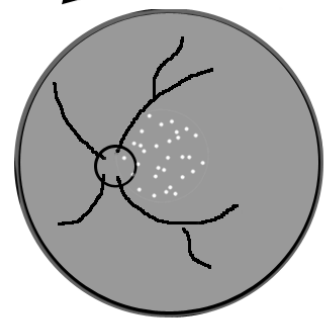
+

$R_{\text{ret_vor}} = 0.5$



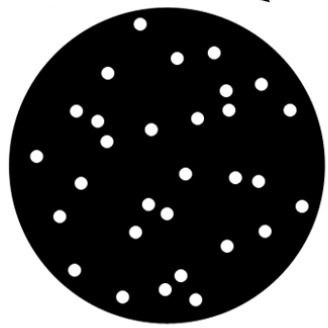
=

$R_{\text{ret_null}} = -1.5$



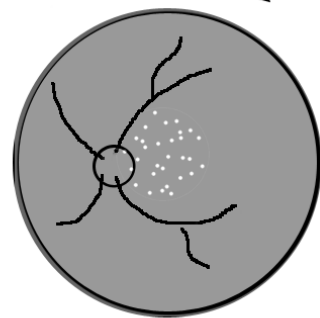
b

$R_{\text{screen_ctrl}} = 1.0$



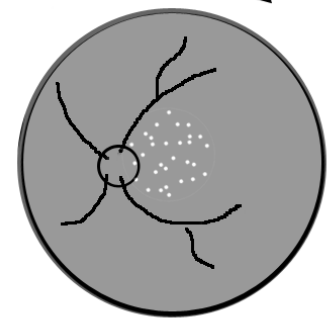
+

$R_{\text{ret_vor}} = 0.5$

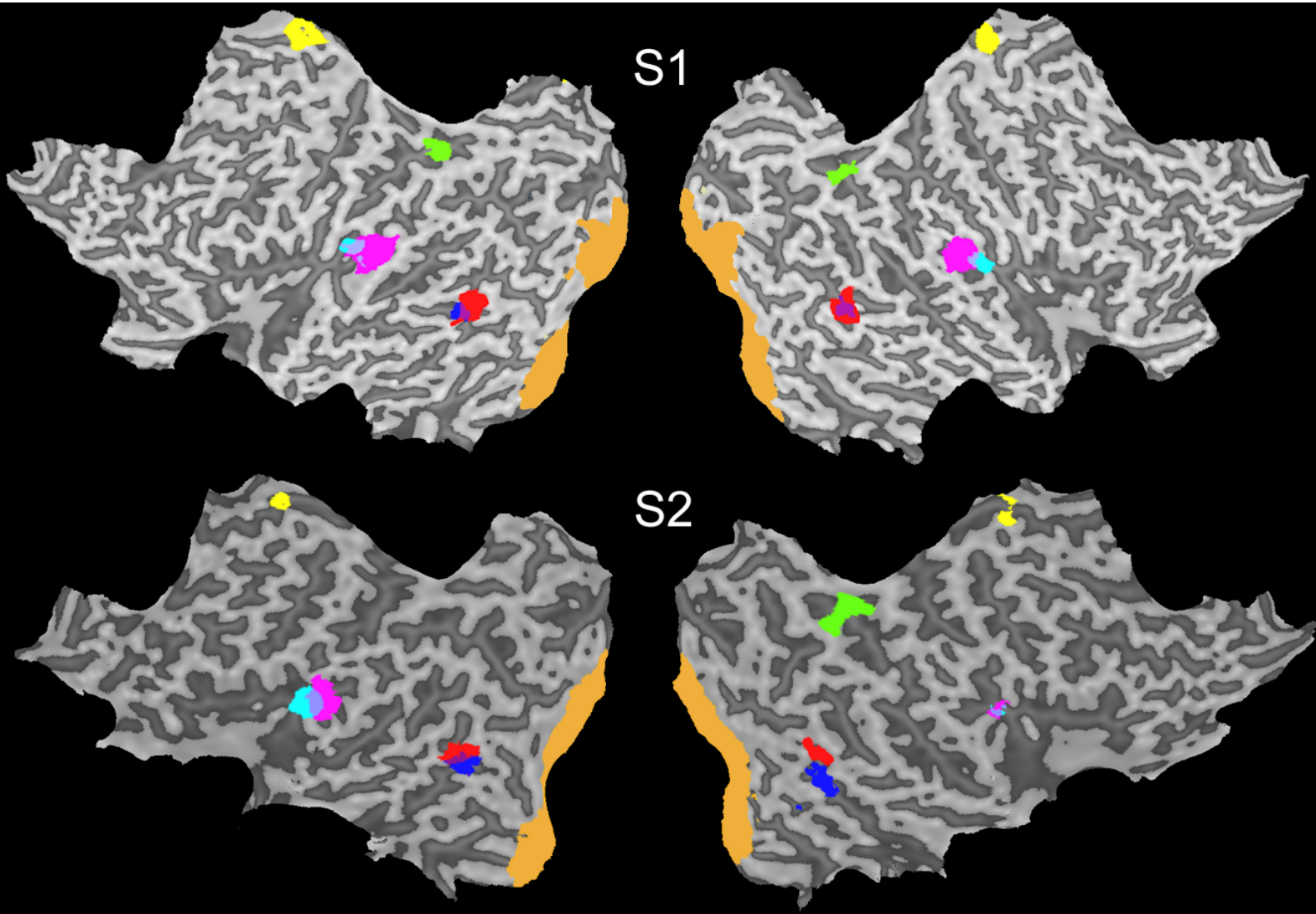


=

$R_{\text{ret_ctrl}} = 1.5$



c



Visual ROIs

hMST ■ pVIP ■ PIC ■ CSv ■ V1 ■

Vestibular ROIs

hMST ■ PIVC/PIC ■

